Investigation of the effects of connectors to enhance bond strength of externally bonded steel plates and CFRP laminates with concrete

Ali Sami Abdul Jabbar [*], Md Ashraful Alam [a] and Kamal Nasharuddin Mustapha [b]

Department of Civil Engineering, Universiti Tenaga Nasional, kajang st. 43000, Malaysia

Abstract. Steel plates and carbon-fiber-reinforced polymer (CFRP) laminates or plates bonded to concrete substrates have been widely used for concrete strengthening. However, this technique cause plate debonding, which makes the strengthening system inefficient. The main objective of this study is to enhance the bond strength of externally bonded steel plates and CFRP laminates to the concrete surface by proposing new embedded adhesive and steel connectors. The effects of these new embedded connectors were investigated through the tests on 36 prism specimens. Parameters such as interfacial shear stress, fracture energy and the maximum strains in plates were also determined in this study and compared with the maximum value of debonding stresses using a relevant failure criterion by means of pullout test. The study indicates that the interfacial bond strength between the externally bonded plates and concrete can be increased remarkably by using these connectors. The investigation verifies that steel connectors increase the shear bond strength by 48% compared to 38% for the adhesive connectors. Thus, steel connectors are more effective than adhesive connectors in increasing shear bond strength. Results also show that the use of double connectors significantly increases interfacial shear stress and decrease debonding failure. Finally, a new proposed formula is modified to predict the maximum bond strength of steel plates and CFRP laminates adhesively glued to concrete in the presence of the embedded connectors.

Keywords: steel plate; CFRP; bond strength; connectors; debonding; concrete

1. Introduction

Many studies have been conducted on the different configurations and techniques for strengthening reinforced concrete beams to prevent or delay the premature debonding of externally bonded (EB) steel plates and carbon fiber-reinforced polymer (CFRP) sheet or strips (Ali *et al*. 2008, Brickner *et al*. 2008, Ceroni *et al*. 2008, Ceroni 2010, Hao *et al*. 2012, Sabahattin *et al*. 2012). However, two known methods are employed to eliminate or minimize premature debonding. The first method is conducted by limiting the ultimate strain at the EB plates. This action was recommended by many dependable design guidelines and standards, such as the American Concrete Institute (ACI) Committee 440-08 (2008), Canadian Standards Association CSA standard

*Corresponding author, Ph.D. Candidate, E-mail: alsami67@gmail.com
[a] Ph.D., Senior lecturer, E-mail: ashraful@uniten.edu.my
[b] Prof. Dr. Acting Deputy Vice-Chancellor, E-mail: kamal@uniten.edu.my

S806-02 (2002), International Federation of Structural Concrete FIB Bulletin-14 (2002), and Japanese Society of Civil Engineers recommendations JSCE (2001), to prevent debonding, which leads to minimize the actual capacities of the bonded steel plates or composites. The second method employs mechanical anchorage (Bank and Arora 2007). Many researchers use different types of local anchorages, such as bolted plates or a fastener gun, to install mechanical fasteners with fender washers through holes in the plates predrilled into the concrete substrate, thus "nailing" the laminates in place (Bank and Arora 2007). Alternatively, some researchers stated that the use of bolt anchorages may initiate cracking in the beams near the bolt holes or cause the brittle rapture failure of bonded plates, which is not a desired mode of failure (Bank and Arora 2007, Lee *et al*. 2009). Thus, many researchers (Smith and Teng 2003, Barros *et al*. 2007, Kim 2009a, b, 2010, Ceroni *et al*. 2008) have recommended the use of a new type of anchorage, namely, fiber-reinforced polymer (FRP) anchorages, which are also known as fan anchors or spikes that are made from FRP fabrics or taw with heads adhesively bonded to external reinforced plates. However, most studies do not focus on understanding the interfacial shear stress and eliminating the debonding failure between the plates and substrate of concrete. One of the most important tests employed to understand interfacial shear stresses is the direct tension pull-out test. Nakaba (Nakaba *et al*. 2001) and Teng *et al*. (2002) conducted this test by using direct tensile force normal to concrete surface (CS), which acts as one shear face, to evaluate the bond stress of bonded plates. Other researchers (Teng *et al*. 2002, Ueda *et al*. 2003) used the double-face shear test, which consist of two bonded plates on opposite faces of concrete prisms (Fig. 1).

The ACI Committee 440 (2008) and Japan Society of Civil Engineers JSCE (2002) recommend the use of direct pull-out test to determine the bond strength of EB plates to concrete. The database contains many pull-out test results of steel plates and CFRP laminates bonded to CS. Dai *et al*. (2005), Luccioni *et al*. (2005), Yao *et al*. (2005), Ren (2003), Zhou (2010) and Biscaia *et al*. (2013) investigated the most effective variables on bond shear stress, such as the effective length (L_e), plate width (b_p), axial stiffness of the plate ($E_p t_p$), and fracture energy (G_f). Most of the above mentioned researchers reported that the compressive strength of the concrete is the most significant factor that affecting the bonding strength because plate peeling or premature debonding occurs in the CS in a layer not exceeding 5 mm beneath the adhesive layer bonding the plate.
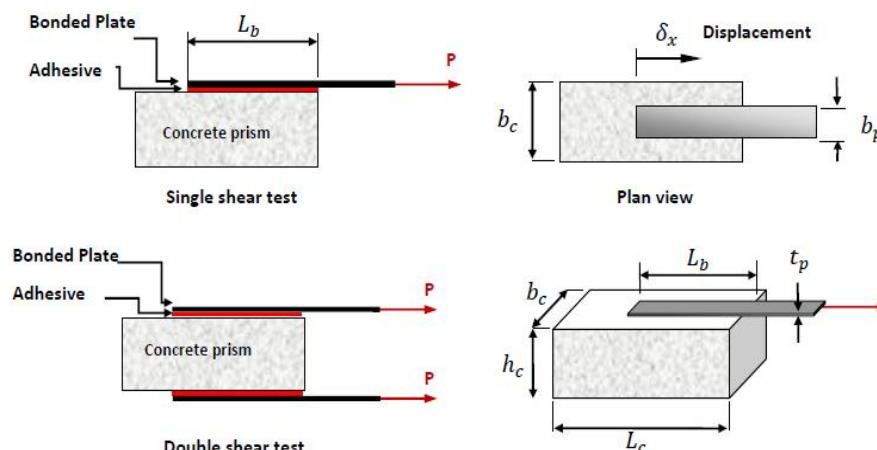

Fig. 1 Pullout test's configuration for single and double lap shear as given by (Teng *et al*. 2002) and (Ueda *et al*. 2003)
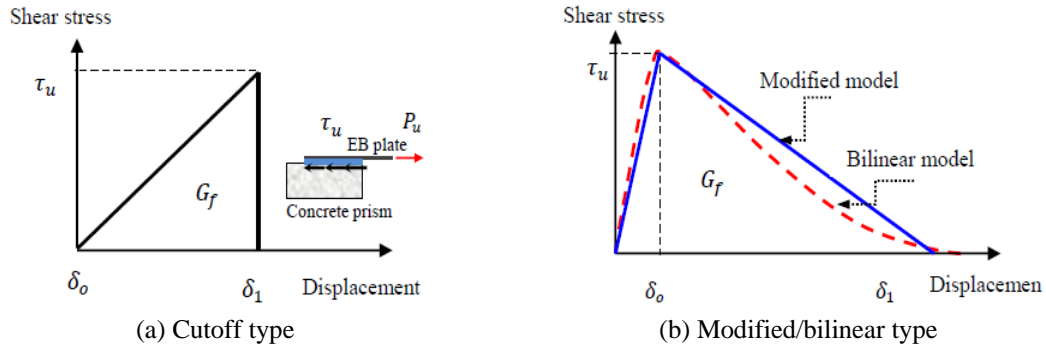
Fig. 2 Local bond-slip relationship from pullout tests as given by (a) cutoff type; (b) bilinear type as given by (Ueda *et al*. 2003) and (Dai *et al*. 2005)

Moreover, the regulations in codes such as ACI Committee 440 (2008), EC-2 (2004), and JSCE (2002), determine the ultimate force P_u as a function of effective bond length, axial stiffness of the bonded plate, and tensile strength of concrete because the previous experimental studies demonstrated that debonding failure occurs at the CS. Consequently, the tensile strength of concrete (f_t) is believed to be one of the main domain variables that affect the debonding phenomena.

The pull-out test not only determines the ultimate load, which is referred to as the bond strength of the steel plate or CFRP laminate to the concrete interface, but also provides better understanding to the local bond–slip behavior of the interface (Yuan *et al*. 2012). The local bond–slip curves from the pull-out tests (Fig. 2) were commonly determined in two ways: (a) from the axial loads on the EB plate measured with closely spaced strain gauges; (b) from the load–displacement curves (Ueda *et al*. 2003).

In general, bond strength models can be classified as analytical models, fracture-based models, and bond–slip models. Predicting the debonding failures by the strength approach methods involves the calculation of the interfacial or bond stress distribution in the plate-strengthened components based on elastic material properties. The calculated stresses are compared with the ultimate strength of the materials to predict the mechanism and load level of debonding failures. These parameters occur as high shear and normal stresses that develop at the ends and at the crack locations of the EB plate. These stresses then lead to interfacial debonding and potential debonding failures. The fracture-based models consider the deformation compatibility condition and provide similar results even though these models exhibit differences in their solution approaches and applicability to various loading configurations. The most reliable models that can be used to calculate the bond strength are the models consider most of the variables that correspond to the fracture energy (G_f), affective bond length (L_e), and axial rigidity of the bonded plate ($E_p t_p$), as well as the concrete compressive strength Ueda (Ueda *et al*. 2003) and Chen and Teng (2001). Therefore, the fundamental formula to predict the bond strength is given as

$$P_u = \sqrt{\frac{2\, E_p\, t_{fp}\, G_f}{1 + \alpha_\tau}}\, b_f \qquad (1)$$

where: $E_p t_p b_p$ are the modulus of elasticity, thickness and width of the bonded plate. G_f is the

fracture energy and α_τ is an aspect ratio related to the bonded plate/laminate and the concrete prism.

Chen and Teng (2001) presented their formula as

$$P_u = 0.427\beta_w\beta_L\sqrt{f_c'}b_p L_e \tag{2}$$

where: f_c' is the concrete compressive strength, L_e is the effective bond length and β_w, β_L are aspect ratios associated with the bonded plate, b_p is the width of the bonded plate.

The effective bond length L_e is defined as the length which is actively involved in the force transfer from the bonded strip to the concrete and is given as

$$L_e = \sqrt{\frac{E_P t_P}{\sqrt{f_c'}}} \tag{3}$$

The aspect ratio of the plates and the concrete prisms is given as

$$\beta_L = \left\{ \begin{array}{l} 1 \; if \; L_e \leq L \\ \sin\dfrac{\pi L}{2L_e} \; if \; L_e > L \end{array} \right\} \tag{4}$$

where: β_w is a factor depends on the width of the bonded plate b_p and the width of the concrete prism b_c.

$$\beta_w = \sqrt{\frac{2 - {b_P}/{b_C}}{1 + {b_p}/{b_c}}} \tag{5}$$

where: β_L is a factor reflects the ratio between the actual bond length L and the effective bond length L_e.

According to previous studies, the behavior of the interface between the EB plates and the exterior surface is the key factor of concrete debonding failures in the external parts of strengthened RC structures. Thus, a consistent understanding of the behavior bonded plate–concrete interfaces must be developed for the safe and economic design of EB plate systems. In this field, a reliable local bond–slip model should be developed to effectively predict debonding failures in externally strengthened RC structures. In this study, the term "interface" is used to refer to the interfacial part of EB plate-to-concrete joint, including the adhesive and a thin layer of adjacent concrete where the relative slip between the bonded plate and the concrete prism occurs instead of any physical interface in the joint. Generally, pure interfacial failure can be identified by the absence of adhesive at the plate surface after failure. Cohesive shear failure can be identified on the basis of the presence of adhesive on both the bonded plate and concrete after failure. Thus, the possible failure of the plates can occur either at the plate–adhesive interface or adhesive–concrete interface. Alternatively, the other failure modes, such as the peeling of FRP or the yielding of steel plates, usually occur in the presence of sufficient anchorage systems. Therefore, in the presence of connectors, the failure mode is believed to be at the plate–adhesive interface because the interfacial shear stress can be transferred deeper inside the sound surface of concrete.

Moreover, the bearing stresses at the connector interface can minimize the debonding problem at the weak concrete–adhesive interface.

To date, research is currently being conducted to determine a dependable design guideline or effective anchoring system to prevent the premature debonding of EB plates used for the shear strengthening of concrete structures. The current study discusses a new method to prevent the premature debonding of steel plates or laminates and experimentally investigates the effect of newly proposed embedded connectors to prevent or delay the shear debonding of EB plates. This work also investigates the efficiency of single/double adhesive and steel connectors in enhancing the interfacial bond strength between the bonded plates and CS.

2. Experimental program

2.1 Test specimens

In this study, 36 reinforced concrete prisms that are 150 mm in width, 150 mm in height, and 350 mm in length were fabricated and divided into 2 series. The first series (PS) of 18 concrete prisms were bonded with steel plates, whereas the second series (PC) were plated with CFRP laminates. The steel plates and CFRP laminates were cut to be 50 mm in width and 350 mm in length and were then fixed on the concrete substrate. The thickness of the steel plate was 2.7 mm, whereas the thickness of the CFRP laminates was 1.2 mm. The bonded area for all the fixed plates was (50 mm × 250 mm) in all cases. Two types of embedded connectors were used, namely, adhesive connectors and steel bar connectors, to enhance the interfacial bond strength. The diameter and depth of all embedded connectors were 30 mm and 25, respectively. For the steel connector, a 16 mm steel bar was inserted in the hole of adhesive filled connectors. Four prisms were strengthened without connectors: 2 prisms for the steel plates and 2 prisms for the CFRP laminates, which were used as control specimens. In each series, 8 specimens were used for adhesive connectors and labeled as the PS-A group. The other 8 specimens were used for steel connectors and labeled as the PS-S group for specimens bonded with steel plates. The same procedure of grouping was employed with prisms plated with CFRP laminates and labeled as PC-A and PC-S for adhesive and steel connectors, respectively. For each group, 4 specimens were fabricated with single connectors and other 4 specimens were fabricated with double connectors. The configuration and details of the specimens are provided in Tables 1A and 1B.

Table 1A Definition of connectors and test specimens bonded with 50 mm wide steel plates

No. of group	Specimen ID	Type of connectors	Bonded area (mm^2)	Connector diameter (mm)	Steel bar diameter (mm)	Effective bonded area (mm^2)
1	PS$_1$-0	No connectors only adhesive at surface	250 × 50	-	-	12500
	PS$_2$-0		250 × 50	-	-	12500
2	PS$_1$-1A	One adhesive connector	Connector area	30	-	706.5
	PS$_2$-1A		Connector area	30	-	706.5
3	PS$_1$-2A	Two adhesive connectors	Connectors area	30	-	1413
	PS$_2$-2A		Connector area	30	-	1413

Table 1A Continued

No. of group	Specimen ID	Type of connectors	Bonded area (mm^2)	Connector diameter (mm)	Steel bar diameter (mm)	Effective bonded area (mm^2)
4	PS$_1$-1S	One 16 mm steel connector	Connector area	30	16	706.5
	PS$_2$-1S		Connector area	30	16	706.5
5	PS$_1$-2S	Two 16 mm steel connector	Connectors area	30	16	1413
	PS$_2$-2S		Connector area	30	16	1413
6	PS$_1$S-1A	One adhesive connector + sur. adhesive	250 × 50	30	-	12500
	PS$_2$S-1A		250 × 50	30	-	12500
7	PS$_1$S-2A	Two adhesive connectors + sur. adhesive	250 × 50	30	-	12500
	PS$_2$-2A		250 × 50	30	-	12500
8	PS$_1$S-1A	One 16 mm steel connector + sur. adhesive	250 × 50	30	16	12500
	PS$_2$S-1A		250 × 50	30	16	12500
9	PS$_1$S-2S	Two 16 mm steel connectors + sur. adhesive	250 × 50	30	16	12500
	PS$_2$S-2S		250 × 50	30	16	12500

Table 1B Definition of connectors and test specimens bonded with 50 mm wide CFRP laminates

No. of group	Specimen ID	Type of connectors	Bonded area (mm^2)	Connector diameter (mm)	Steel bar diameter (mm)	Effective bonded area (mm^2)
1	PC$_1$-0	No connectors only adhesive at surface	250 × 50	12500	-	-
	PC$_2$-0		250 × 50	12500	-	-
2	PC$_1$-1A	One adhesive connector	Connector area	706.5	-	30
	PC$_2$-1A		Connector area	706.5	-	30
3	PC$_1$-2A	Two adhesive connectors	Connectors area	1413	-	30
	PC$_2$-2A		Connector area	1413	-	30
4	PC$_1$-1S	One 16 mm steel connector	Connector area	706.5	16	30
	PC$_2$-1S		Connector area	706.5	16	30
5	PC$_1$-2S	Two 16 mm steel connector	Connectors area	1413	16	30
	PC$_2$-2S		Connector area	1413	16	30
6	PC$_1$S-1A	One adhesive connector + sur. adhesive	250 × 50	12500	-	30
	PC$_2$S-1A		250 × 50	12500	-	30
7	PC$_1$S-2A	Two adhesive connectors + sur. adhesive	250 × 50	12500	-	30
	PC$_2$-2A		250 × 50	12500	-	30
8	PC$_1$S-1A	One 16 mm steel connector + sur. adhesive	250 × 50	12500	16	30
	PC$_2$S-1A		250 × 50	12500	16	30
9	PC$_1$S-2S	Two 16 mm steel connectors + sur. adhesive	250 × 50	12500	16	30
	PC$_2$S-2S		250 × 50	12500	16	30

Table 2 Mix proportions of concrete

Materials	Kg/m^3
Water	205
Cement	315
Fine aggregate ($d < 5$ mm)	1116
Coarse aggregate ($5 < d < 20$ mm)	744
Slump ratio	65-120 mm

2.2 Preparation of concrete prisms

The reinforcement cages of 6 mm steel bars were made for each specimen to avoid any shrinkage cracks in the prisms. The compressive strength of the concrete was designed to be in the range of 35 MPa. The entire concrete prisms for both types of connectors were mixed, poured into steel molds, and externally vibrated. After 24 hours, the specimens were de-molded and cured for 28 days. The prisms were stored at laboratory temperature for 2 months until testing. The mixing design is indicated in Table 2. Twelve concrete cylinders with 150 mm in diameter and 300 mm in height were fabricated and arranged for compression, splitting, tensile strength, and modulus of elasticity tests to represent the properties of the concrete. On the day of testing the mean compressive strength of concrete was found to be 30,5 MPa, the tensile strength of concrete f_t was 3.1 MPa, splitting strength f_{ctm} was 2.7 MPa and Young's modulus of the concrete E_c was 30.85 GPa.

2.3 Connector's preparation and fixing the plates

The connector's holes were drilled using an electric drill machine. The depths of the connector holes were fixed in the range of 25 mm. The adhesive connectors were made of holes filled with adhesive only. The adhesive was spread along the perimeter of the connector by using a steel stick. Prisms with adhesive connectors of 30 mm in diameter were fabricated as a single connector and double connectors with a spacing of 100 mm between the drilled holes (Figs. 3 and 4). The steel connectors were fabricated by drilling 30 mm-diameter holes filled with adhesive and inserting 16 mm steel bars inside them. The steel bars were prepared by cutting a normal flexural reinforcement bar to fixed pieces with 25 mm length. The steel bars were mounted inside the 30 mm-diameter holes (Fig. 5). Sikadur-30 epoxy adhesive was mixed using a mechanical mixer according to the manufacture's specification and then placed inside the connectors. The steel bars were well spread on the bonding zone at the CS by steel scraper. Steel plates that are 50 mm in width, 350 mm in length, and approximately 2.7 mm in thickness were sandblasted with quartz sand and positioned in the middle of the prism. The yield strength of the steel plate used was 275 MPa, and the modulus of elasticity was 200 MPa. Table 3 indicates the properties of the materials employed in this study. The top surface of the concrete prisms was peeled off by scaling hammer to expose the aggregates and improve the grip between the adhesive and plate. The plates were then glued to the top surface of the prisms by using a 2 mm-thick layer of epoxy adhesive. The steel plate was placed 50 mm far from each side of the specimen (Fig. 6). In this arrangement, the interface behavior between the steel plates and concrete was not influenced by the edge peeling effect. All strengthened specimens with the bonded steel plates were cured at room temperature for one week before testing.
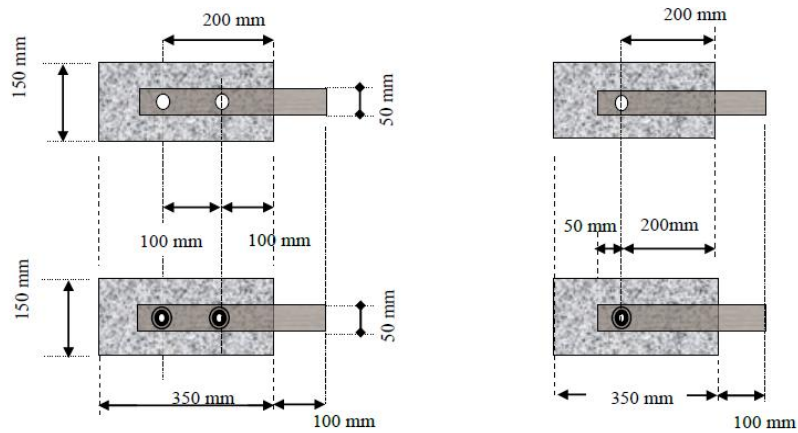
Fig. 3 Prisms fabricated with single and double connectors (adhesive connectors and 16 mm steel bar connectors) without adhesive on surface
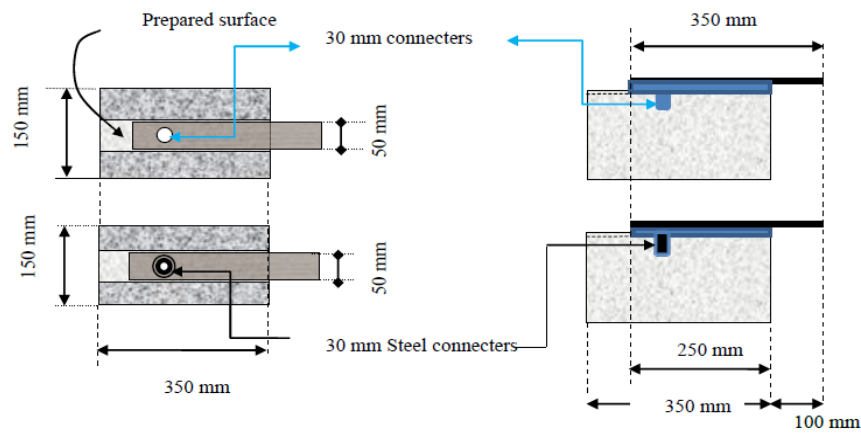

Fig. 4 Prisms fabricated with single connector (adhesive and 16 mm steel bar connectors) in addition to adhesive on surface of 250 mm length
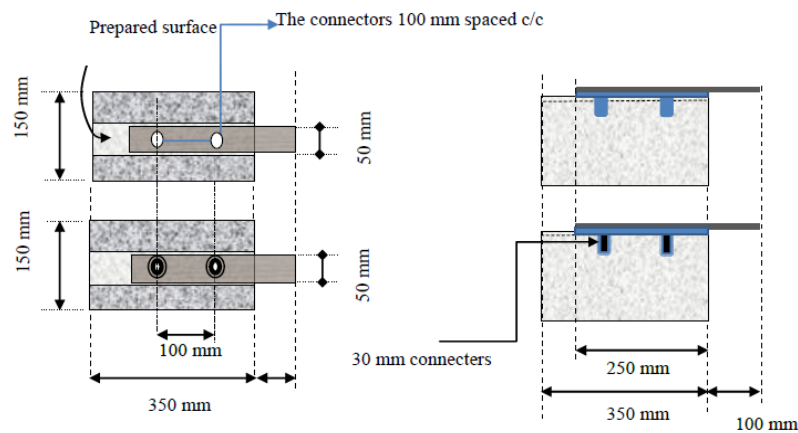

Fig. 5 Prisms fabricated with double connectors (adhesive and 16 mm steel bar connectors) in addition to adhesive on surface of 250 mm length

Table 3 Material properties

Prisms	Concrete	(Adhesive Sikadure-30)	CFRP laminates	Steel plates
$b = 150$ mm	$f_c' = 30\ MPa$	$f_a = 70\ MPa$	$t_{pc} = 1.2\ mm$	$t_p = 2.7\ mm$
$h = 150$ mm	$E_c = 30.56\ GPa$	$E_a = 12880\ GPa$	$E_p = 165\ GPa$	$E_s = 200\ GPa$
$L = 350$ mm	$f_t = 2.7$	$f_t = 5.1$	$f_t = 1260\ MPa$	$f_y = 275\ MPa$ $f_t = 320\ MPa$

Fig. 6 Steel plates bonded to the concrete prisms for the pull-out test

3. Test setup

3.1 Testing procedure

On the basis of the recommendations of Australian Standards (HB 305- 2008), single-lap shear tests were established for all strengthened specimens. Fig. 7 shows the arrangement and fabrication of the pull-out rig that was used in this experiment and was similar to the previously mentioned single-lap tension tests.

Assuming that the frames of the rig prevent the concrete prism from up-lifting, the width and thickness of each of the three components (plate, adhesive layer, and concrete prism) are constant. According to the previous considerations, a simple mechanical model for the pull-out shear test can be established by treating the plate and concrete prism (the two adherents) as subject to axial deformations only, whereas the adhesive layer can be assumed to be subject to shear deformations only. Hence, both adherents are assumed to be subject to uniformly distributed axial stresses with any bending effects neglected, whereas the adhesive layer is assumed to be subject to shear stresses that are constant across the thickness of the adhesive layer.

The steel rig was made of two 15 mm-thick upper and lower steel plates and four 15mm rods with nuts and washers. The load was applied vertically by a hydraulic jack of the UTM tension machine with an increment of approximately 1 kN per minute. A supporting frame was adjusted under the grip plate to minimize the out-of-plane loading in all directions. According to (HB 305-2008), the gap between the upper corner of the reaction plate and bonded surface of the steel plate should be minimized to prevent any bending effect. The grip in this experimental work was maintained at 100 mm because of the previously mentioned reasons. A positioning frame was applied to maintain the specimen in the right place and prevent the far end of the concrete prisms from moving upwards during the pull-out test.
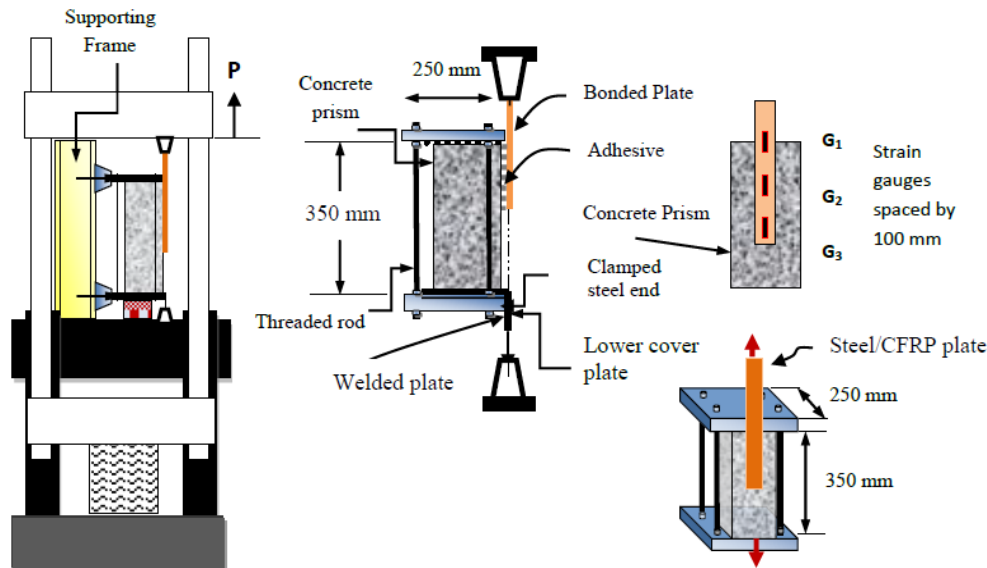
Fig. 7 Arrangement of the steel rig for single lap pull-out test

3.2 Instrumentation

The strain of the bonded plates was measured by using three strain gauges fixed at the beginning of the bond-free part of the plate and the other strain gauges with a space of 100 mm (Fig. 7). The displacement was also measured by using the LVDT placed between the load cell and prism. Direct tension tests were conducted by the UTM machine, and the load was monitored by using a load cell connected to the data logger. The load cell, LVDT, and strain gauge wires are connected to a data acquisition system (Fig. 7).

4. Experimental results

4.1 Effects of connectors to enhance bond strength

In the first series of prisms bonded with steel plates, two control specimens without shear connectors with normal bonded steel plates were tested to determine the behavior of the bond strength between the steel plate and concrete prisms. When the control specimen was tested, the failure crack in the adhesive was visible when the load approached 24 kN, followed by the debonding of the steel plate when the load approaches 26 kN. Two control prisms from the second series for specimens with CFRP laminates without connectors reached an average debonding load of 26.17 kN. No cracks were observed before the debonding failure. The specimens with single connectors alone without adhesive on surface that bond steel plates were also tested to investigate the bond strength capacity of a single adhesive and steel bar connectors. The average bond strengths of the adhesive connector and single-steel connector were approximately 15.9 and 17.9 kN, respectively. The same testing procedure was conducted for the specimens of single adhesive and steel connectors that bond CFRP laminates. The average bond strength was 15.2 and 16.2 kN. The experiment results for the specimens fabricated with single connectors combined with
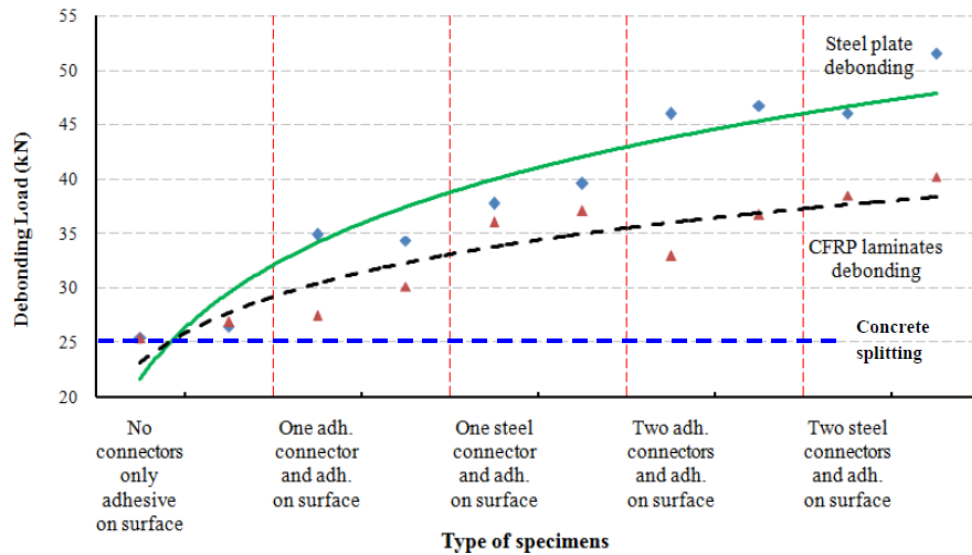
Fig. 8 Effect of connectors to enhance the bond strength

Table 4A Test results for specimens bonded with steel plates using (adhesive or steel) connectors

Specimen ID	Type of connectors	Bonded load (kN)	Average debonding load (kN)	Ultimate shear stress (MPa)	Displace -ment δ_1 (mm)	Mode of failure
PS$_1$-0	No connectors only	25.426	26.0	2.034	0.24	Concrete peeling
PS$_2$-0	adhesive surface	26.465		2.117		
PS$_1$-1A	One adhesive connector	16.020	15.87	22.6/Conn.	0.15	Connector splitting
PS$_2$-1A		15.720		22.2/Conn.		
PS$_1$-2A	Two adhesive connectors	26.206	24.89	18.5/Conn.	0.23	Steel plate slipping at connector joint
PS$_2$-2A		23.574		17/Conn.		
PS$_1$-1S	One 16 mm steel connector	17.015	17.94	24/Conn	0.17	Steel plate slipping at connector joint
PS$_2$-1S		18.862		26.7/Conn		
PS$_1$-2S	Two 16 mm steel connector	31.383	32.7	22.2/Conn.	0.31	Steel plate slipping at connector joint
PS$_2$-2S		34.017		24/Conn.		
PS$_1$S-1A	One adhesive connector + Adhesive on surface	34.867	34.6	2.789	0.32	Concrete peeling
PS$_2$S-1A		34.34		2.747		
PS$_1$S-2A	Two adhesive connectors + Adhesive on surface	45.975	46.36	3.678	0.429	Concrete peeling &Yield of steel plate
PS$_2$-2A		46.749		3.740		
PS$_1$S-1A	One 16 mm steel connector + Adhesive on surface	37.734	38.65	3.019	0.35	Concrete peeling & Yield of steel plate
PS$_2$S-1A		39.576		3.166		
PS$_1$S-2S	Two 16 mm steel connectors + Adhesive on surface	46.002	48.751	3.68	0.45	Concrete peeling & Yield of steel plate
PS$_2$S-2S		51.500		4.12		

Table 4B Test results for specimens bonded with CFRP laminates using (adhesive or steel) connectors

Specimen ID	Type of connectors	Debonding load (kN)	Average debonding load (kN)	Ultimate shear stress (MPa)	Displace-ment δ_1 (mm)	Mode of failure
PC$_1$-0	No connectors only adhesive surface	25.426	26.173	2.034	0.660	Concrete peeling + CFRP splitting
PC$_2$-0		26.920		2.154		
PC$_1$-1A	One adhesive connector	14.754	15.247	20.9/Conn.	0.385	CFRP splitting
PC$_2$-1A		15.740		22.2/Conn.		
PC$_1$-2A	Two adhesive connectors	21.758	23.692	15.4/Conn.	0.590	Connector peeling + CFRP splitting
PC$_2$-2A		25.625		18.13/Conn.		
PC$_1$-1S	One 16 mm steel connector	16.054	16.281	23/Conn	0.410	Connector peeling + CFRP splitting at connector joint
PC$_2$-1S		16.507		23.4/Conn		
PC$_1$-2S	Two 16 mm steel connector	29.122	29.871	20.6/Conn.	0.754	Connector peeling + CFRP splitting at connector joint
PC$_2$-2S		30.619		21.3/Conn.		
PC$_1$S-1A	One adhesive connector + Adhesive on surface	27.456	28.800	2.196	0.730	Concrete peeling + CFRP splitting
PC$_2$S-1A		30.141		2.411		
PC$_1$S-2A	Two adhesive connectors + Adhesive on surface	32.944	34.822	2.63	0.880	Concrete peeling + CFRP splitting
PC$_2$-2A		36.699		2.94		
PC$_1$S-1A	One 16 mm steel connector + Adhesive on surface	36.047	36.546	2.88	0.92	Concrete peeling + CFRP splitting
PC$_2$S-1A		37.051		2.96		
PC$_1$S-2S	Two 16 mm steel connectors + Adhesive on surface	40.234	39.367	3.2	0.98	Concrete peeling + CFRP splitting
PC$_2$S-2S		38.512		3.1		

Table 5A Failure modes of specimens bonded with steel plate using single (adhesive or steel) connector
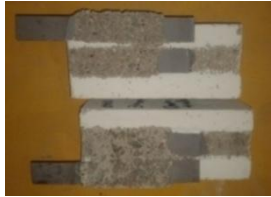
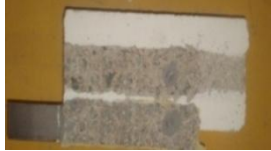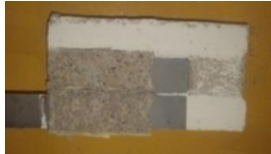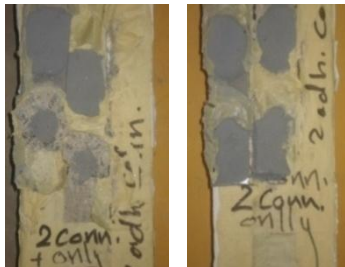| No. of group	Type of connector	The prisms of single connectors profile	Maximum strain in plate	Failure mode
1	One adhesive connector		0.00056	Adhesive shear failure at the connector's joint with an arbitrary ring of concrete around the connector peeled off
2	One 16 mm steel connector		0.00066	Adhesive shear failure at the adhesive-plate interface

Table 5A Continued

No. of group	Type of connector	The prisms of single connectors profile	Maximum strain in plate	Failure mode
3	One adhesive connector + adhesive on surface		0.00128	Shear failure at concrete surface combined with adhesive layer attached to the plate upon the connector joint
4	One 16 mm steel connector + adhesive on surface		0.00136	Shear failure at concrete surface with 5 mm concrete layer attached to the plate combined with steel plate yielding
5	One 16 mm steel connector + adhesive on surface		0.00143	2nd type of failure peeling of 5 mm layer under the adhesive and slip of plate above connector's joint (yield of the steel plate)

250 mm adhesive on the surface exhibited debonding loads P_u of 34.6 and 38.66 kN for both single adhesive and steel connectors respectively. Therefore, the increment was found to be 34 % and 48 % compared to the control prisms. The results are given in Tables 4A and 4B and the range of the increasing in the specimen's bond strength is shown in (Fig. 8). The comparisons of the load capacities for specimens bonded with steel plates and CFRP strips are shown in Figs. 9-14. The applied load and relative displacement between the EB plates and concrete prisms were monitored during the experiments as given in Tables 4A and 4B. The mode of failure of the samples is presented in Tables 5-6.

Table 5B Failure mode of specimens bonded with steel plate using double (adhesive or steel) connectors
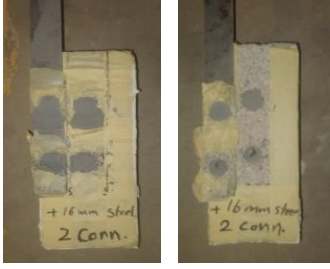
No. of group	Type of connector	The prisms of single connectors profile	Maximum strain in plate	Failure mode
1	Two adhesive connectors		0.0009	Adhesive shear failure at the connector's joint, other samples show peeling of an arbitrary ring of concrete around one joint

Table 5B Continued

No. of group	Type of connector	The prisms of single connectors profile		Maximum strain in plate	Failure mode
2	Two 16 mm steel connectors			0.0012	Adhesive shear failure at the connector's joint, and peeling of an arbitrary ring of concrete around one joint
3	Two adhesive connectors + adhesive on surface			0.0017	Crushing of the concrete combined with yielding of steel plate
4	Two 16 mm steel connectors + adhesive on surface			0.002	Slipping of the plate at the adhesive-plate interface and crushing of the concrete's edges combined with yielding of steel plate

4.2 Effects of number of connectors to enhance bond strength

Double connector prisms without adhesive at the surface show higher bond resistance and debonding load than single connector prisms. Moreover, prisms with a double connector combined with 250 mm adhesive on surface exhibit a maximum debonding load of 51 kN. The steel plate started to yield when the load reached 35 kN. When the load reached 51 kN the specimen exhibited crushing of the upper end of the concrete prism followed by full separation of the steel plate. Thus, the experimental observations indicate that the double connector system can effectively delay premature debonding and change the failure mode to ductile mode rather than sudden brittle debonding because the steel plate starts to yield before reaching the final failure. All test specimens with double steel connectors exhibited higher debonding load P_u than the specimens with double adhesive connectors. Therefore, double embedded steel connectors are more efficient than double adhesive connectors Tables 4A and 4B. The effect of doubling the connectors for specimens with steel plates is shown in Figs. 9 and 10. Moreover, the same effect can be observed in specimens with CFRP laminates, as indicated in Figs. 11 and 12.

Table 6 Failure modes of specimens plated with CFRP using (adhesive or steel) connector

No. of group	Type of connector	The prisms of single connectors profile	Maximum strain in plate	Failure mode
1	Control no connectors		0.0029	Concrete peeling and partial CFRP laminate splitting
2	One adhesive connector		0.00127	Shear failure at plate adhesive interface and slip of CFRP laminate above connector's joint
3	One 16 mm steel connector		0.0014	Shear failure at plate adhesive interface and slipping of the CFRP laminate above the connector joint
4	One adhesive + adhesive on surface		0.003	Shear failure at plate adhesive interface and slipping of plate above connector's joint
5	One 16 mm steel connector + adhesive on surface		0.0031	Shear failure at plate adhesive interface and slipping of plate above connector's joint
6	Two adhesive connectors + adhesive on surface		0.0035	Splitting of the CFRP laminate
7	Two 16 mm steel connectors + adhesive on surface		0.004	Splitting of the CFRP laminate

Effect of number of connectors
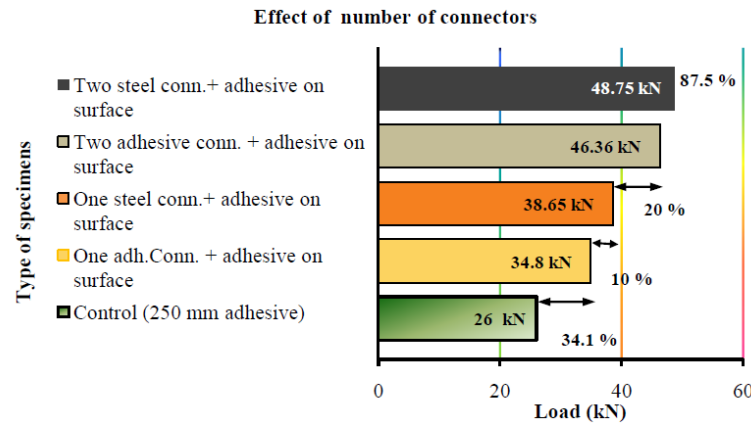

Fig. 9 Effect of increasing number of connectors of prisms plated with 50 mm wide steel plates using 250 mm adhesive on surface
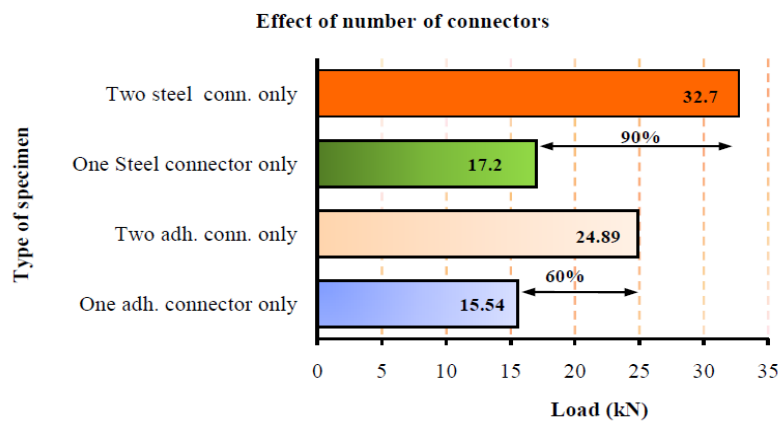
Effect of number of connectors

Fig. 10 Effect of increasing the number of connectors for prisms plated with 50 mm wide steel strips without using adhesive on surface

Effect of number of connectors
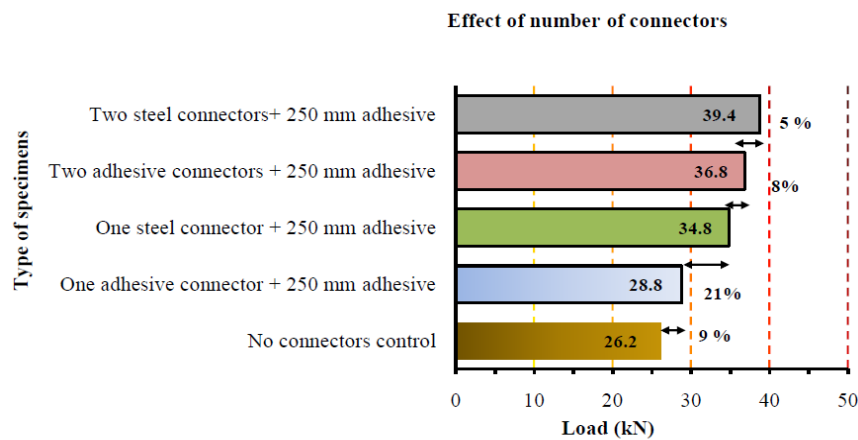

Fig. 11 Effect of increasing the number of connectors of prisms plated with 50 mm wide CFRP strips using 250 mm adhesive on surface
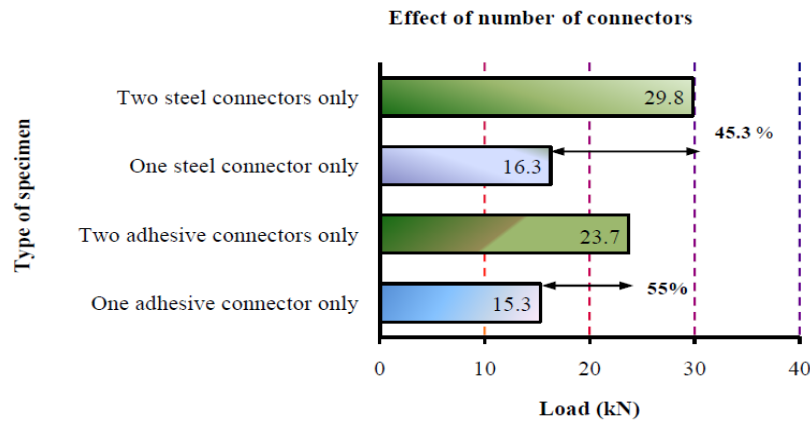
Effect of number of connectors

Fig. 12 Effect of increasing the number of connectors of prisms plated with 50 mm wide CFRP strips without using adhesive on surface

4.3 Effect of the type of connector

Both connectors prevented the premature debonding failure of bonded plates. However, the investigation indicates that the highest capacity of shear strengthening is reached when embedded steel connectors are utilized. The failure in the prisms with steel connectors exhibited slipping of the plate at the adhesive surface, which tends to produce higher splitting strength than concrete because the splitting strength of the steel plate to the adhesive was 5.1 MPa compared with 2.9 MPa for concrete to the adhesive interface. Moreover, the bearing capacity of the steel bar inside the connector hole is higher than that of the adhesive. Thus, the steel connectors not only performed better than the adhesive connectors to enhance the bonding strength but are also economical. The comparison between the types of connectors for the specimen with steel plates is shown in (Fig. 13). Fig. 14 indicates the effect of the type of connector for specimens with CFRP strips. The failure modes of both connectors are presented in Tables 5 and 6.

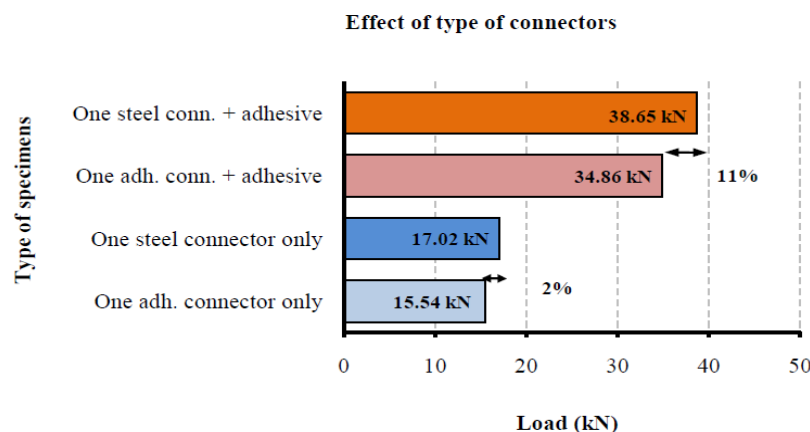**Effect of type of connectors**

Fig. 13 Effect of type of connector for prisms bonded with 50 mm wide steel plates using single (adhesive or steel) connector
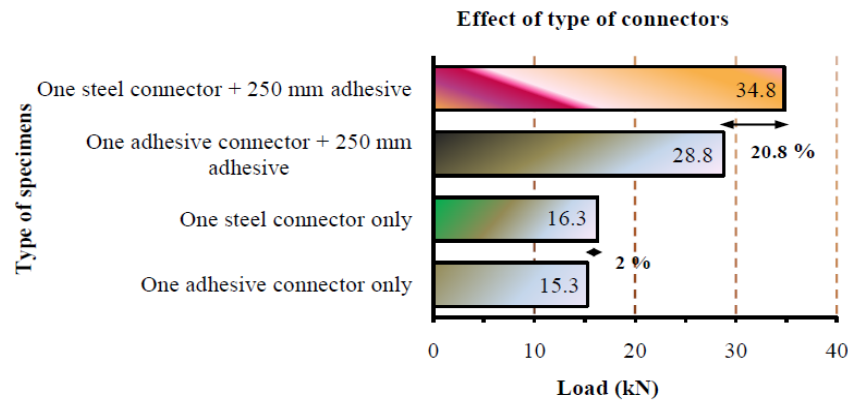
Fig. 14 Effect of type of connector for prisms plated with 50 mm wide CFRP strips using single (adhesive or steel) connector
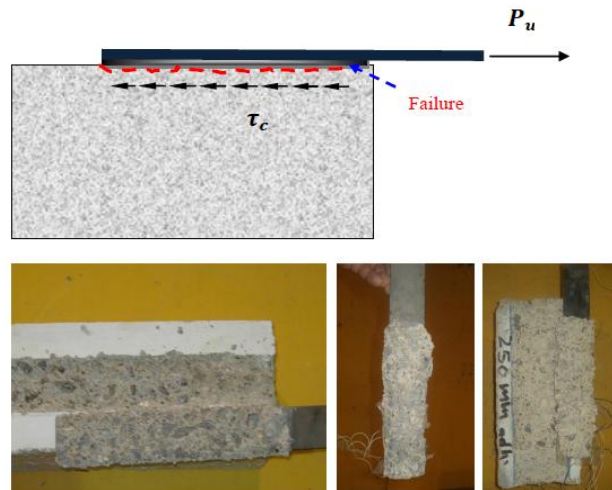

Fig. 15 Failure modes of prisms without connectors presented by peeling of 5 mm thickness from concrete surface beneath the bonded plate

4.4 Failure modes of specimens in the presence of connectors

The steel plate exhibited debonding at the concrete–adhesive interface because of excessive interfacial shear stress. The bond strength of concrete is lower than the bond strength of adhesive. Thus, debonding occurs at the CS nearly 5 mm beneath the adhesive (Fig. 15). On the basis of the connectors, the failure mode will be at the plate–adhesive interface because the interfacial shear stress can be transferred inside the prism. Moreover, the bearing stresses at the connector interface can minimize the debonding problem at the concrete–adhesive interface Figs. 16 and 17.

The experiments also indicate that the failure mode differs from brittle sudden debonding in the control samples without connectors because failure occurs inside the CS. The failure of the samples with adhesive connectors is less brittle than those with steel connectors, and the failure line occurs in the interfacial surface of the adhesive (between the steel plate and adhesive) on the
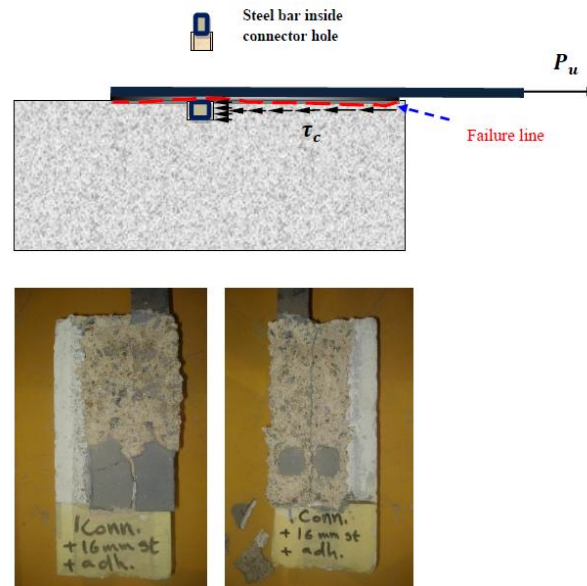
Fig. 16 Failure modes of prisms with embedded connector presented by concrete peeling and splitting of the plate at the connector joint
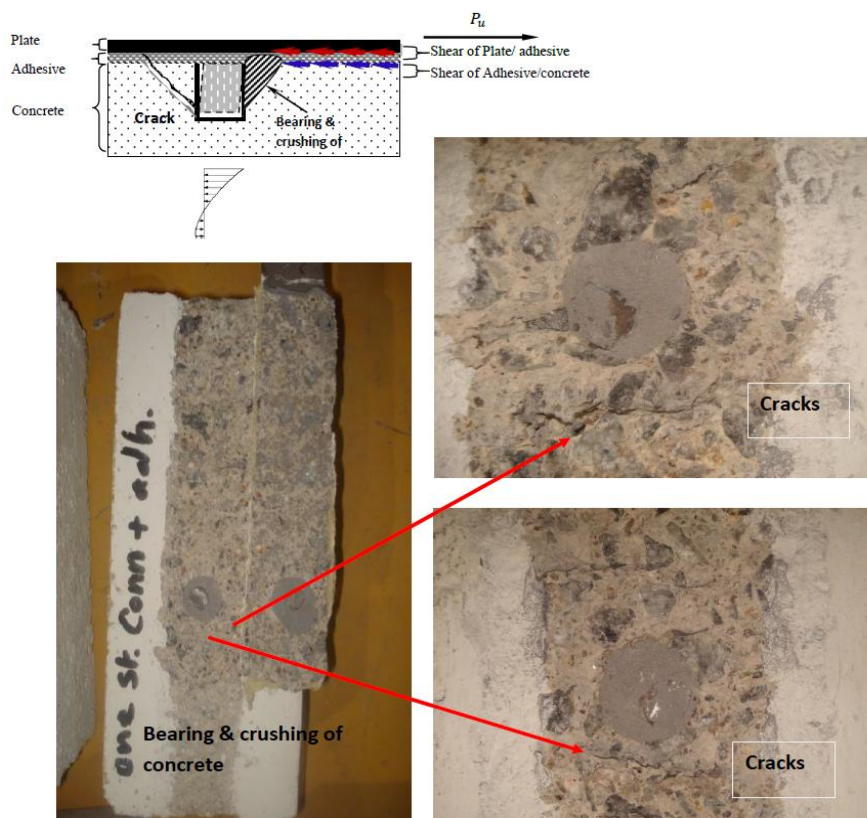

Fig. 17 Effect of the steel connectors presented by cracks inside the concrete surface due to bearing stress

connector area when the new connectors transfer the stresses effectively inside the concrete. The same failure occurs in the remaining steel connector specimens that failed at the adhesive surface joint (between the bonded plate and adhesive) when the adhesive strength is exceeded (Fig. 17).

4.5 Distribution of shear strain on connectors

The strain gauge readings at various load levels for steel-to-concrete joints are presented in Figs. (18-20). Strain gauge G1 refers to the strain in the end loaded point of the plate, whereas the readings of G2 and G3, which were spaced 100 mm apart, represent the strains in the bonded joints. On the basis of these strain distribution profiles, three distinct profile trends correspond to three different regions of the joint may be identified depending on the level of loading. The first trend corresponds to the exponentially decreasing strain distributions when load is initially applied. This exponential trend extends over the region between gauges G1 and G3. The distance required for the strain to reach zero defines the $\delta_o - \delta_1$, which is called the initial transfer length. Once a crack is initiated, a further increase in loading gradually displaces the transfer region toward the
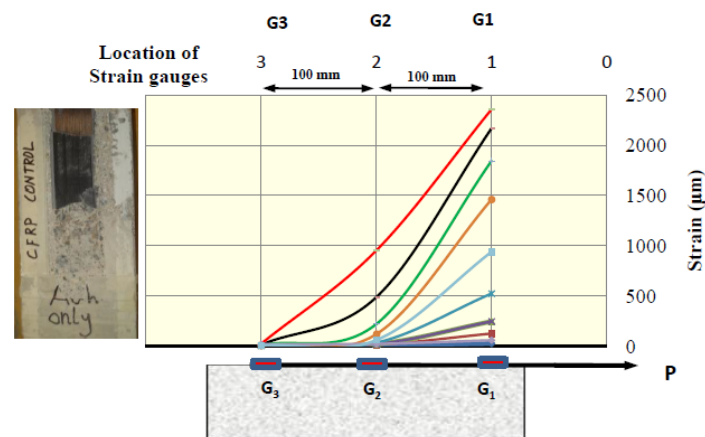

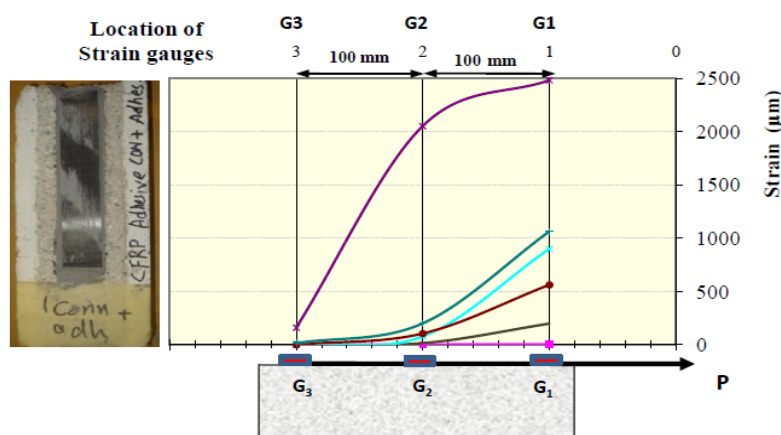Fig. 18 Strain distribution for prisms plated with CFRP strips without connectors

Fig. 19 Typical strain distribution for prisms plated with CFRP strips with single adhesive connector
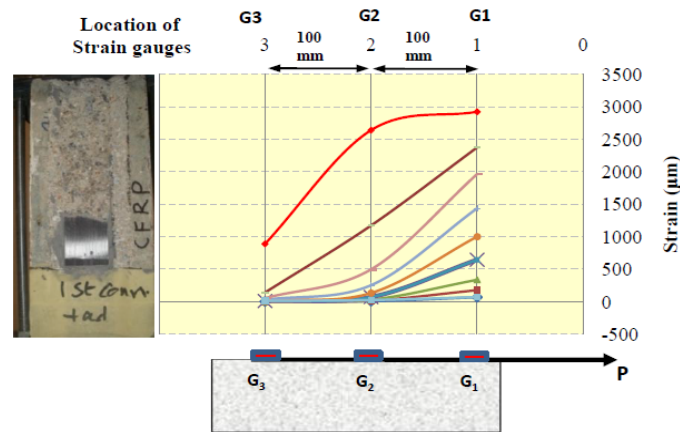
Fig. 20 Typical strain distribution for prisms plated with CFRP strips with steel connector

unloaded end. The resulting strain profiles show a more or less bilinear decreasing trend with a transition point occurring at the limit of the initial transfer region. This transition point coincides with either gauge G2 or G3. On one hand, strain compatibility does not seem to occur, particularly close to the failure in the normal bond of the plates without connectors (control prisms). On the other hand, the strain compatibility in the prisms with embedded connectors seems to prevent the concentration of the stresses at the plate end. Figs. 19-20 indicate that the strain was nearly similar at the middle and end of the plate surface attached to the adhesive before debonding failure occurs. The connectors significantly transfer interfacial shear stresses because the bearing stress inside the concrete reduces the concentration of the interfacial shear strain of the end plate, thus minimizing the debonding of the EB plates.

5. A Proposed model to predict the ultimate bond strength of steel plate and CFRP laminate in presence of connectors

The fundamental equations of shear stress distribution lengthwise the bonded plates and attributed fracture energy can be derived as follows

$$G_f = \frac{1}{2}\,\tau_u\,\delta_1 \tag{6}$$

where G_f the fracture energy assumed to be the area under the bond shear (τ)– slip (δ) curve and τ_u is the ultimate shear stress between the bonded plate and the concrete and is given as

$$\tau_u = \frac{P_u}{b_p L_b} \tag{7}$$

where L_b is the actual bonded length. The maximum tensile stress in the bonded plate is given as

$$\sigma_t = E_p.\varepsilon_u \tag{8}$$

where ε_u is the ultimate strain at the plate's end for maximum displacement.

Therefore, the maximum displacement is given as

$$\delta_1 = \frac{\sigma_t}{E_p}.L_b = \frac{P_u/(A_p)}{E_p}.L_b \tag{9}$$

where A_n is the actual bonded area under the plate presented by the width of the plate b_p and the bonded length L_b.

From Eqs. (6) and (9) we can calculate the fracture energy from

$$G_f = \frac{P_u^2}{2b_p^2 E_p t_p} \tag{10}$$

Therefore, the fundamental equation to predict the ultimate bond strength P_u is given as

$$P_u = b_p \sqrt{2G_f E_p t_p} \tag{11}$$

where E_p, t_p and b_p are the modulus of elasticity, thickness and width of the bonded plate.

To provide a model for predicting the ultimate bond strength of the steel plate and CFRP strips externally glued to the concrete surface in the presence of connectors, a simple analysis was made using the existing experimental results. The contribution from the new connectors was added by superposition to the main formula presented in Eq. (11), which is similar to the formula given by the Italian code (2004), [CNR-200 Guide for Design and Construction]. Therefore, the new model is basically depending on the fracture energy Mode II, which was experimentally calculated in the presence of the connectors and shown in (Fig. 21). Therefore, the proposed equation is given as

$$P_u = 0.75.\ b_p \sqrt{\frac{2G_f E_p t_p}{(1 + \alpha_t)}\frac{L}{L_e}\left(2 - \frac{L_b}{L_e}\right)} \quad \text{if} \quad L_b < L_e \tag{12}$$
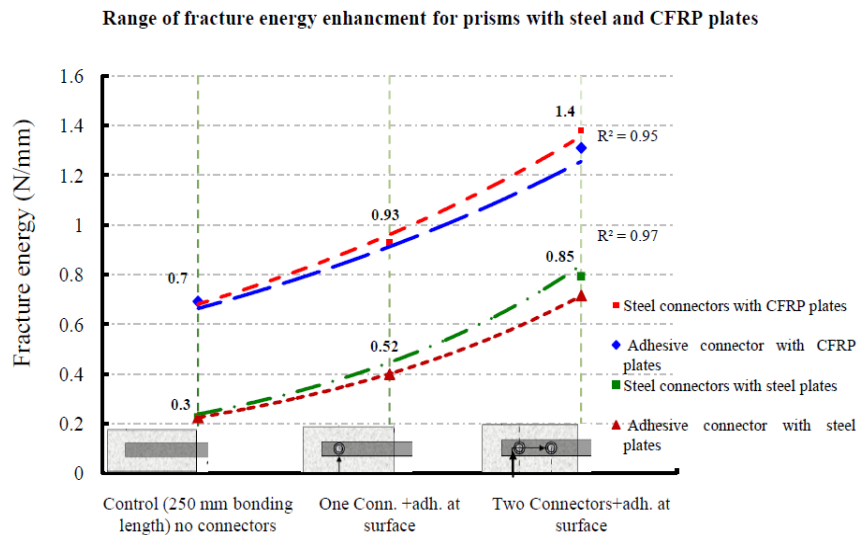

Fig. 21 Effect of increasing the number of connectors on the fracture energy G_f

$$P_u = 0.75 \, b_p \sqrt{\frac{2G_f E_p t_p}{(1 + \alpha_t)}} \quad \text{if} \quad L_b > L_e \tag{12a}$$

where L_b: is the actual bonded length, G_f: is the fracture energy in the presence of connectors. The calculated fracture energy G_f was found to be in the range 0.5 for steel plates and 1.2 N/mm for CFRP laminates. The calculated fracture energy is given in Table 7.

The effective bond length L_e and can be calculated in same manner given in Eq. (3).

α_t: is a ratio related to the axial rigidity of the concrete prism and the bonded strip and given as

$$\alpha_t = \frac{E_p t_p b_p}{E_c t_c b_c} \tag{12b}$$

Table 7 Calculated fracture energy and predicted debonding loads

| Type of connector	Type of the bonded plate	Fracture energy G_f (N/mm)	$P_{u \ Test}$ tested debonding load (kN)	$P_{u \ Pred.}$ predicted debonding load (kN)	$\dfrac{P_{u \ Predicted}}{P_{u \ Tested}}$
Control no connectors	Steel plate	0.250	26	25.8	0.99
One adhesive connector	Steel plate	-	15.8	14.1	0.89
One 16 mm steel connector	Steel plate	-	17.9	16.2	0.91
Two adhesive connector	Steel plate	-	24.9	28.2	1.1
Two16 mm steel connector	Steel plate	-	32.7	32.4	0.99
One adhesive + adh. on surface	Steel plate	0.444	34.6	34.2	0.99
One 16 mm steel connector + adh. on surface	Steel plate	0.554	38.6	37.2	0.96
Two adhesive connectors + adh. on surface	Steel plate	0.796	46.4	45.4	0.97
Two 16 mm steel connectors + adh. on surface	Steel plate	0.881	48.8	49.5	1.01
Control no connectors	CFRP laminates	0.680	26.1	25.8	0.98
One adhesive connector	CFRP laminates	-	15.2	14.1	0.92
One 16 mm steel connector	CFRP laminates	-	16.3	16.2	1
Two adhesive connector	CFRP laminates	-	23.7	28.2	1.18
Two16 mm steel connector	CFRP laminates	-	28.8	32.4	1.12
One adhesive + adh. on surface	CFRP laminates	0.840	29.8	32.6	1.09
One 16 mm steel connector + adh. on surface	CFRP laminates	1.300	34.8	33.8	0.97
Two adhesive connectors + adh. on surface	CFRP laminates	1.350	36.6	38	1.03
Two 16 mm steel connectors + adh. on surface	CFRP laminates	1.560	39.4	40.1	1.01
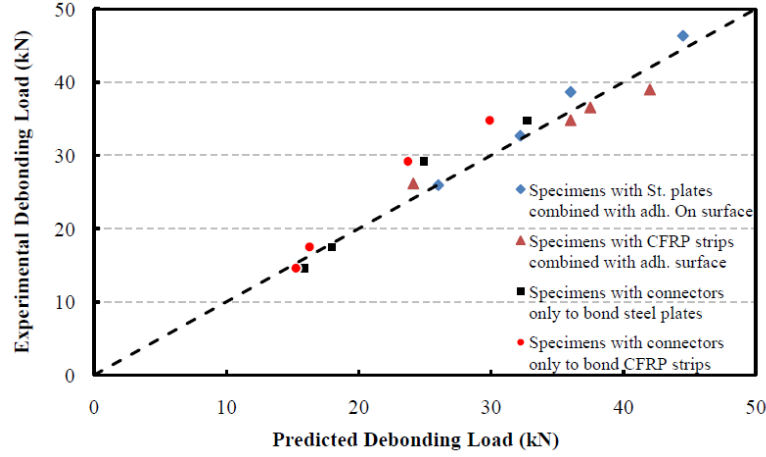
Fig. 22 Ratio between the predicted debonding load and the tested debonding load

where: $E_p t_p b_p$ are the modulus of elasticity, thickness and the width of the bonded plate. E_c, t_c and b_c is the concrete modulus of elasticity, height of prism and width of prism respectively and L_b is the actual bond length.

The contribution provided by the connector as shear strength is given as

$$F_{A.Conn.} = \tau_{A.Conn.} . \pi \left(\frac{D_{Conn.}^2}{4} \right) . \frac{D_{Conn.}}{b_p} \quad \text{for Adhesive conn.} \tag{13}$$

$$F_{S.Conn.} = \tau_{S.Conn.} . \pi \left(\frac{D_{Conn.}^2}{4} \right) . \frac{D_{Conn.}}{b_p} \quad \text{for Steel conn.} \tag{14}$$

$\tau_{A.Conn.}$:   Average shear stress provided by adhesive connector.
$\tau_{S.Conn.}$:   Average shear stress provided by steel connector.
$D_{Conn.}$:   Diameter of connector
b_p: Plate width

The contribution provided by the connector as bearing strength is given by

$$F_B = 0.57 . A_s . n . \sqrt{f_c'} . \frac{D_{conn.}}{b_p} < 1.5 \text{ kN} \tag{15}$$

F_B: Average local bearing strength provided from each connector, *n* is the number of connectors, is the compressive strength of concrete and A_s is the cross sectional area of the embedded connector.

The predicted debonding loads based on the proposed equations were found to be very close with the experimental findings. The ratios between the predicted and the tested values are given in Table 7 and shown in (Fig. 22).

6. Conclusions

The investigation shows that the use of new embedded connectors effectively delays the premature debonding of the steel plate and CFRP laminates. The new connectors enhance the bond strength and prevent the concentration of the interfacial stress at the ends of the fixed plates, which are assumed to be the main reason to cause the premature debonding failure.

Using single connector increased the bond strength by 48% and 38% for specimens bonded with steel plates and CFRP strips respectively. Additionally, using double connectors increased the bond strength by 84% and 53% for specimens bonded with steel plates and CFRP strips respectively. Both the measured maximum displacement value and maximum steel plate strain values are significantly higher for prisms with embedded connectors compared to prisms without connectors. The measured maximum strain values in strips bonded with steel connector were higher than that in strips bonded with adhesive connector, thus resulting in a significantly improved performance. All steel plates bonded to prisms using double connectors exhibited yielding before debonding.

The failure modes were different in prisms with connectors than that in prisms without connectors because the bonded plate separated at the plate–adhesive interface rather than at the concrete–adhesive interface, which is assumed to be the weakest plane in the system. In the case of specimens with CFRP strips, the efficiency of the embedded connectors leads to the splitting of the CFRP plates.

The capacity of the steel connectors to enhance the interfacial bond strength was found to be higher than the adhesive connectors by 25% for prisms plated with CFRP strips and by 35% for prisms bonded with steel plates. The investigation showed that the steel connectors are more capable of establishing sufficient connection capacity to allow the bonded plates to undergo large plastic deformation, which leads to increased ductility at failure.

The fracture energy in specimens with double connectors was found to be two times higher than the specimens with single connector for both steel plates and CFRP strips. The maximum fracture energy reached was 1.6 N/mm, in specimens with double connectors, while it was only 0.25 N/mm for control specimens without connectors.

It was found that the proposed equation gives comparable predictions with the experimental results and yet conservative over the range of variables known to affect the bond strength. Further work is needed to investigate the efficiency of the proposed embedded connectors with other materials, which are traditionally in use for external shear strengthening of RC beams now days.

Acknowledgments

References

ACI 440.2R (2008), Guide for the Design and Construction of Externally Bonded FRP Systems for Strengthening Concrete, Reported by ACI Committee 440.

Ali, M.M., Oehlers, D.J., Griffith, M.C. and Seracino, R. (2008), "Interfacial stress transfer of near surface-mounted FRP-to-concrete joints", *Eng. Struct.*, **30**(7), 1861-1868.

Aykac, S., Kalkan, I. and Uysal, A. (2012), "Strengthening of reinforced concrete beams with epoxy-bonded perforated steel plates", *Struct. Eng. Mech., Int. J.*, **44**(6), 735-751.

Bank, L.C. and Arora, D. (2007), "Analysis of RC beams strengthened with mechanically fastened FRP (MF-FRP) strips", *Compos. Struct.*, **79**(2), 180-191.

Barros, J.A., Dias, S.J. and Lima, J.L. (2007), "Efficacy of CFRP-based techniques for the flexural and shear strengthening of concrete beams", *Cement Concrete Compos.*, **29**(3), 203-217.

Biscaia, H.C., Chastre, C. and Silva, M.A. (2013), "Linear and nonlinear analysis of bond-slip models for interfaces between FRP composites and concrete", *Compos. Part B: Eng.*, **45**(1), 1554-1568.

Brückner, A., Ortlepp, R. and Curbach, M. (2008), "Anchoring of shear strengthening for T-beams made of textile reinforced concrete (TRC)", *Mater. Struct.*, **41**(2), 407-418.

Canadian Standards Association (CAN) (2002), CSA-S806-02: Design and construction of building components with fibre-reinforced polymers, Canadian Standards Association; Mississauga, ON, Canada.

Ceroni, F. (2010), "Experimental performances of RC beams strengthened with FRP materials", *Construct. Build. Mater.*, **24**(9), 1547-1559.

Ceroni, F., Pecce, M., Matthys, S. and Taerwe, L. (2008), "Debonding strength and anchorage devices for reinforced concrete elements strengthened with FRP sheets", *Compos. Part B: Eng.*, **39**(3), 429-441.

Chen, J.F. and Teng, J.G. (2001), "Anchorage strength models for FRP and steel plates bonded to concrete", *J. Struct. Eng.*, **127**(7), 784-791.

Dai, J., Ueda, T. and Sato, Y. (2005), "Development of the nonlinear bond stress–slip model of fiber reinforced plastics sheet–concrete interfaces with a simple method", *J. Compos Construct.*, **9**(1), 52-62.

EC 2-1 (2004), Eurocode 2: Design of concrete structures – Part 1: Common rules for building and civil engineering structures; prEN 1992-1, CEN (Comité Européen de Normalisation), European Committee for Standardisation, Central Secretariat, Brussels, Belgium.

FIB Bulletin 14 (2002), Externally bonded FRP reinforcement for RC structures; Task group 9.3, International Federation of Structural Concrete (FIB).

Hao, S.W., Liu, Y. and Liu, X.D. (2012), "Improved interfacial stress analysis of a plated beam", *Struct. Eng. Mech., Int. J.*, **44**(6), 463-478.

HB 305-2008 (2008), Design handbook for RC structures retrofitted with FRP and metal plates: Beams and slabs; Standards Australia: 476, Sydney, NSW 2001, Australia, 68 p.

JSCE (2001), Japan Society of Civil Engineers: Recommendations for upgrading of concrete structures with use of continuous fiber sheets, Concrete Engineering Series, No. 41, Tokyo, Japan, 250 p.

Kim, S.J. and Smith, S.T. (2009a), "Behaviour of handmade FRP anchors under tensile load in uncracked concrete", *Adv. Struct. Eng.*, **12**(6), 845-865.

Kim, S.J. and Smith, S.T. (2009b), "Shear strength and behavior of FRP spike anchors in cracked concrete", *Proceedings of the 9th International Symposium on Fiber Reinforced Polymer Reinforcement for Concrete Structures*, FRPRCS-9: Sydney, Australia.

Kim, S.J. and Smith, S.T. (2010), "Pullout strength models for FRP anchors in uncracked concrete", *J. Compos. Constr.*, **14**(4), 406-414.

Lee, J.H., Lopez, M.M. and Bakis, C.E. (2009), "Slip effects in reinforced concrete beams with mechanically fastened FRP strip", *Cement Concrete Compos.*, **31**(7), 496-504.

Luccioni, B.M., López, D.E. and Danesi, R.F. (2005), "Bond-slip in reinforced concrete elements", *J. Struct. Eng.*, **131**(11), 1690-1698.

Nakaba, K., Kanakubo, T., Furuta, T. and Yoshizawa, H. (2001), "Bond behavior between fiber-reinforced polymers laminates and concrete", *ACI Struct. J.*, **98**(3), 359-367.

Ren, H.T. (2003), "Study on basic theories and longtime behavior of concrete structures strengthened by fiber reinforced polymers", Ph.D. Thesis; University of Technology, Dalian, China.

Smith, S.T. and Teng, J.G. (2002), "FRP-strengthened RC structures-II: assessment of debonding strength models", *Eng. Struct.*, **24**(4), 397-417.

Smith, S.T. and Teng, J.G. (2003), "Shear-bending interaction in debonding failures of FRP-plated RC

beams", *Adv. Struct. Eng.*, **6**(3), 183-199.

Teng, J.G., Zhang, J.W. and Smith, S.T. (2002), "Interfacial stresses in reinforced concrete beams bonded with a soffit plate: A finite element study", *Construct. Build. Mater.*, **16**(1), 1-14.

Teng, J.G., Smith, S.T., Yao, J. and Chen, J.F. (2003), "Intermediate crack-induced debonding in RC beams and slabs", *Construct. Build. Mater.*, **17**(6), 447-462.

Ueda, T., Dai, J.G. and Sato, Y. (2003), "A nonlinear bond stress-slip relationship for FRP sheet–concrete interface", *Proceedings of the International Symposium on Latest Achievement of Technology and Research on Retrofitting Concrete Structures*, Volume 11320, pp. 113-120.

Yao, J., Teng, J.G. and Chen, J.F. (2005), "Experimental study on FRP-to-concrete bonded joints", *Compos.-Part B: Eng.*, **36**(2), 99-113.

Yuan, H., Lu, X., Hui, D. and Feo, L. (2012), "Studies on FRP-concrete interface with hardening and softening bond-slip law", *Compos. Struct.*, **94**(12), 3781-3792.

Zhou, Y.W., Wu, Y.F. and Yun, Y. (2010), "Analytical modeling of the bond–slip relationship at FRP-concrete interfaces for adhesively-bonded joints", *Compos. Part B: Eng.*, **41**(6), 423-433.

CC

Appendix

From the test it was found that Young's modulus of concrete, $E = 30$ GPa, poison ratio v for concrete is 0.3. The maximum splitting stress f_t of concrete can be found from the formula

$$f_t = 0.5\sqrt{f_c'} = 0.5 \times \sqrt{30} = 2.74 \text{ MPa}$$

The average shear stress (bond stress in this case) can be calculated by

$$\tau_{avg.} = \frac{V_{bond}}{A}$$

where; A is the boded area of plate.

$$A = b_p \times L_b = 50 \times 250 = 12500 \text{ mm}^2$$

So the maximum shear stress should be not exceeding the splitting shear stress.

$$\tau_{avg} \leq f_t \leq 2.74 \text{ MPa}$$

$$2.74 = \frac{V_{bond}}{A} = \frac{V_{bond}}{10000}$$

Max, $V_{bond} = 33.7$ kN (if no connectors are provided)

$$L_e = \text{effctive length}$$

$$L_b = 250 \text{ mm the actual bond length}$$

$$b_P = 50 \text{ mm the plate width,}$$

$$t_P = 2.7 \text{ mm the plate thickness}$$

$$E_P = 200 \text{ MPa the steel plate modulus of elasticity}$$

Therefore $\beta_P = 1.118$, $\beta_w = 1$

$$P_u = 0.427 \times 1.118 \times 1 \times \sqrt{30}X50 \times 200 = 26.148 \text{ kN} \text{ (Chen and Teng 2001)}$$

To calculate the capacity of single adhesive and steel connectors the excesses of the bond force can be calculated as follows

$$F_{A.Conn.} = \frac{P_u}{A_{Conn.}} = \frac{16020}{\frac{\pi(30)^2}{4}} = 22 \text{ MPa for adhesive connector}$$

$$F_{S.Conn.} = \frac{P_u}{A_{Conn.}} = \frac{17015}{\frac{\pi(30)^2}{4}} = 24MPa \text{ for steel connector}$$

Since

$$L_e = \sqrt{\frac{200000. \times 2.7}{\sqrt{30}}} = 314 \text{ mm} > 200 \text{ mm the actual bond length}$$

Therefore the ultimate bond strength for in presence of single adhesive connector is given from second equation as

$$P_u = 0.75 \times (50)\sqrt{\frac{2(0.5 \times 200000 \times 2.7)}{1.14}} \times \left(\frac{250}{316}\right) \times \left(2 - \frac{250}{314}\right)$$

$$+ 22 \times 1 \times \pi \times \left(\frac{30^2}{4}\right) \times \frac{30}{50} + 0.57 \times 30 \times 25 \times \sqrt{30} \times \frac{30}{50} = 34.2 \; kN.$$

Notation

P_u	:	Ultimate bond strngth
G_f	:	Mode (II)Fracture energy
b_p	:	Bonded plate width
E_p	:	Modulus of elasticity of bonded plate
E_c	:	Modulus of elasticity of concrete prism
t_p	:	Steel plate thickness
t_c	:	Concrete prism thickness
f_t	:	Tensile strength
f_{ctm}	:	Splitting strength of concrete
f_c	:	Compresive strength of concrete
f_y	:	Yield strength of steel
L_b	:	Actual bond length
L_e	:	Effective bond length
n	:	Number of connectors
σ_b	:	Maximum bond stress
α_t	:	ratio of the axial rigidity for both concrete and steel plate
$F_{A.Conn.}$	:	Shear stress provided by adhesive connector
$F_{S.Conn.}$	:	Shear stress provided by steel connector
$F_{Bearing}$	:	Local bearing stress provided by each connector